J Biomol NMR (2015) 61:311–320
DOI 10.1007/s10858-014-9876-5

ARTICLE

Solid-state NMR, electrophysiology and molecular dynamics characterization of human VDAC2

Zrinka Gattin · Robert Schneider · Yvonne Laukat · Karin Giller · Elke Maier · Markus Zweckstetter · Christian Griesinger · Roland Benz · Stefan Becker · Adam Lange

Received: 19 September 2014 / Accepted: 11 November 2014 / Published online: 16 November 2014

Abstract The voltage-dependent anion channel (VDAC) is the most abundant protein of the outer mitochondrial membrane and constitutes the major pathway for the transport of ADP, ATP, and other metabolites. In this multidisciplinary study we combined solid-state NMR, electrophysiology, and molecular dynamics simulations, to study the structure of the human VDAC isoform 2 in a lipid bilayer environment. We find that the structure of hVDAC2 is similar to the structure of hVDAC1, in line with recent investigations on zfVDAC2. However, hVDAC2 appears to exhibit an increased conformational heterogeneity compared to hVDAC1 which is reflected in broader solid-state NMR spectra and less defined electrophysiological profiles.

Keywords Voltage-dependent anion channel · Membrane proteins · Solid-state NMR · Molecular dynamics simulations

Introduction

Voltage-dependent anion channels (VDACs) are 30–35 kDa pore-forming proteins located in the mitochondrial outer membrane (MOM) (Sorgato and Moran 1993). They are involved in regulation of metabolite flux of ions and small metabolites like ATP/ADP (Benz 1994; Rostovtseva and Colombini 1997) between mitochondria and the cytosol, and they also have been implicated in the mitochondrial pathway of apoptosis. From its first

Z. Gattin · R. Schneider · Y. Laukat · K. Giller · M. Zweckstetter · C. Griesinger · S. Becker · A. Lange
Max Planck Institute for Biophysical Chemistry, Am Fassberg 11, 37077 Göttingen, Germany

Z. Gattin
Max Planck Institute for Dynamics and Selforganisation, Am Fassberg 17, 37077 Göttingen, Germany

R. Schneider
Unité de Glycobiologie Structurale et Fonctionnelle, Université des Sciences et Technologies de Lille, Bât. C9, 59655 Villeneuve d'Ascq, France

E. Maier · R. Benz
Lehrstuhl für Biotechnologie, Theodor-Boveri-Institut (Biozentrum) der Universität Würzburg, Am Hubland, 97074 Würzburg, Germany

M. Zweckstetter
Deutsches Zentrum für neurodegenerative Erkrankungen (DZNE), Göttingen, Germany

M. Zweckstetter
Center for the Molecular Physiology of the Brain, University Medical Center, 37073 Göttingen, Germany

R. Benz
School of Engineering and Science, Jacobs University Bremen, Campusring 1, 28759 Bremen, Germany

A. Lange (✉)
Leibniz-Institut für Molekulare Pharmakologie (FMP), Robert-Rössle-Str. 10, 13125 Berlin, Germany
e-mail: alange@fmp-berlin.de

A. Lange
Institut für Biologie, Humboldt-Universität zu Berlin, Invalidenstr. 110, 10115 Berlin, Germany

discovery in 1976 (Schein et al. 1976) to date, multiple VDAC isoforms have been identified in a variety of organisms, including yeast, plants, mouse, and humans (Smack and Colombini 2014; Colombini 1980; Lindén and Gellerfors 1983; Blachly-Dyson et al. 1993). In mammals, three VDAC isoforms (VDAC1, VDAC2, and VDAC3) have been identified, with variable expression in all tissues (Sampson et al. 1996, 2001).

In 2008, the structures of murine and human VDAC1 were solved using NMR, combined X-ray and NMR, and pure X-ray methods (Hiller et al. 2008; Bayrhuber et al. 2008; Ujwal et al. 2008). All structures unambiguously revealed a novel barrel topology of 19 ß-strands with an N-terminal α-helical region situated within the aqueous pore. While the three structures slightly differ in location and length of the N-terminal helix, we could show that in a native-like lipid bilayer environment, the N-terminal region of human VDAC1 assumes a well-defined conformation containing a kinked α-helix, similar to that of the murine VDAC1 structure (Schneider et al. 2010). The structure of the N-terminal part of VDAC1 was also shown to depend on the environment (De Pinto et al. 2007).

The fundamental properties of all VDACs in all eukaryotic kingdoms are highly preserved, although some studies revealed important differences in the regulatory functions within the different cell types. These studies strongly indicate functional specialization rather than redundancy between the three VDAC isoforms (Blachly-Dyson and Song 1997; Sampson et al. 2001). Biochemical studies of the mammalian VDACs have revealed that all three isoforms display similar channel-forming activity, and each can compensate for deficiency of the others (Sampson et al. 1997; Anflous et al. 2001). However, genetic studies have shown that VDAC2 knockout mice are embryonic lethal, whereas both VDAC1 and VDAC3 knockout mice are viable (Anflous et al. 2001; Sampson et al. 2001; Cheng et al. 2003), suggesting that VDAC2 fulfils functions different from VDAC1 and VDAC3. In contrast to VDAC1, VDAC2 and VDAC3 are found to play a more prominent role in cell death. VDAC2 is known as a specific inhibitor of BAK-dependent mitochondrial apoptosis (Cheng et al. 2003) and is required for the pro-apoptotic activity of BAX in the absence of BAK (Yamagata et al. 2009). Furthermore, the nonapoptotic mechanism of cell death mediated by the anti-tumor agent erastin involves VDAC2 and VDAC3, but not VDAC1 (Yagoda et al. 2007; Bauer et al. 2011).

VDAC1, the most abundant isoform among the three mammalian VDACs, has continuously been investigated in the past decade; see e.g. (Villinger et al. 2014) for a recent study. In contrast, biological data for VDAC2 have become available only in recent years which indicated that this isoform retains a different functionality from VDAC1 (Sampson et al. 2001; Cheng et al. 2003). However, neither extensive experimental nor computational investigations had been performed that could provide structural and functional information on the hVDAC2 isoform at the atomic level. The first attempt to tackle the hVDAC2 structure with solution NMR was reported in 2012 by Yu et al. (2012). In contrast to hVDAC1, hVDAC2 presented itself to be of low stability when embedded in LDAO detergent micelles, which was only slightly improved by incorporation into DMPC nanodiscs, so that sequence-specific assignments for only 50 % of backbone amide resonances were feasible. The situation changed in 2014 with the work by Abramson and coworkers (Schredelseker et al. 2014) who reported the successful X-ray structure determination of zebra fish (zf) VDAC2. The overall structure of zfVDAC2 was found in this study to be highly similar to the structure of hVDAC1.

Although the N-terminal region of hVDAC2 is eleven amino acids longer than the one of hVDAC1, the part where the α-helix is expected in hVDAC2 has more than 90 % sequence similarity with hVDAC1. Thus it seems likely that the N-terminal part of hVDAC2 adopts a similar conformation as in the hVDAC1 structure (see Fig. 1). The role of the first eleven residues of hVDAC2 remains unclear. Some studies indicated that it is superfluous for its function (Naghdi et al. 2012), while others suggested the full-length version of VDAC2 to be more functional than a shortened version (without residues 1–11) (Reina et al. 2010). Unfortunately, the structure reported by Schredelseker et al. (2014) cannot provide any evidence to this matter as zfVDAC2 lacks the first eleven amino acids in the N-terminal part.

Our main interest in this study was on structural similarities and differences between hVDAC1 and hVDAC2 in a lipid bilayer setting at the atomic level and on functional differences that may arise from different structures. Of particular interest were the N-terminal parts of hVDAC1 and hVDAC2.

In parallel to experimental studies on VDAC, several molecular dynamics (MD) based studies have been performed, but until now only with the VDAC1 isoform mostly focusing on its ion permeability and selectivity (Krammer et al. 2011; Rui et al. 2011; Zachariae et al. 2012; Teijido et al. 2014; Choudhary et al. 2014). So far no computational studies have been conducted on the VDAC2 isoform.

In this multidisciplinary study where we combined solid-state NMR methods, electrophysiology studies and molecular dynamics simulations, we show that the structure of hVDAC2 in a lipid bilayer environment is similar to the structure of hVDAC1. However, hVDAC2 appears to exhibit an increased conformational heterogeneity compared to hVDAC1 which is reflected in broader solid-state NMR spectra and less defined electrophysiological profiles.

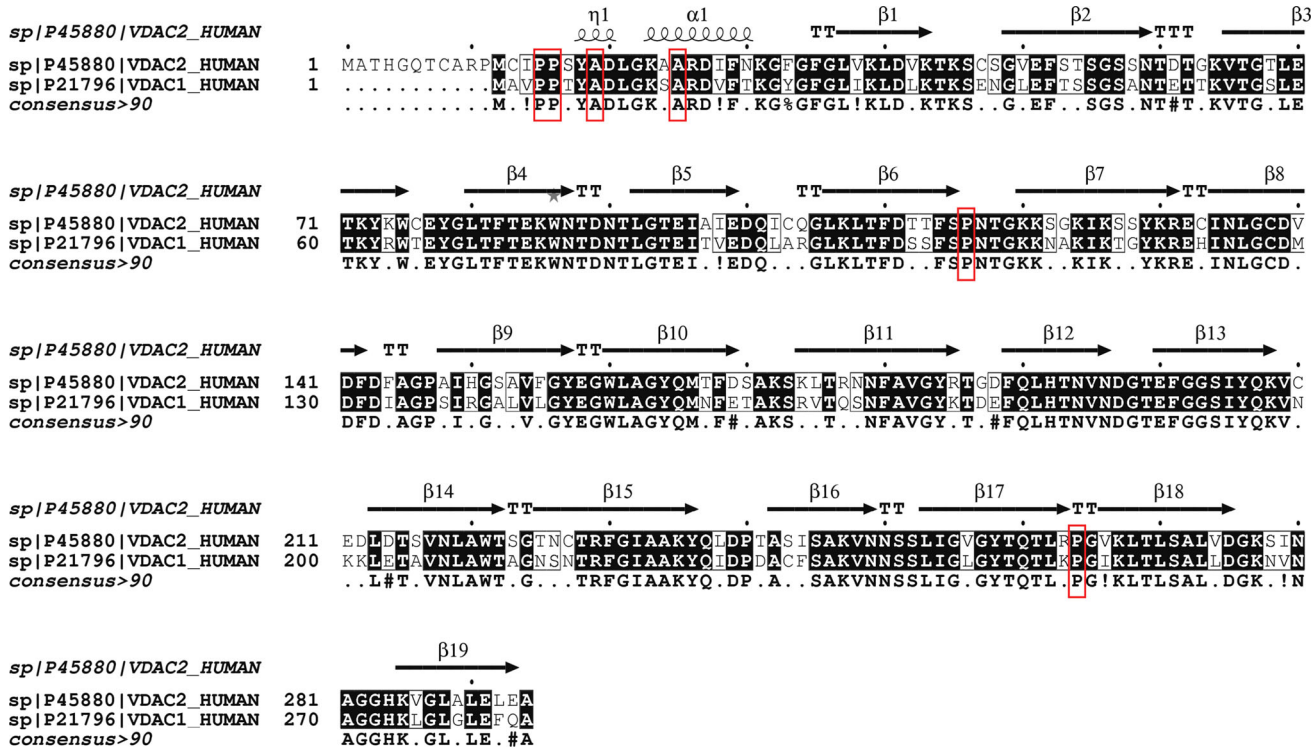

Fig. 1 Sequence alignment between human VDAC1 and VDAC2. The sequence alignment was performed with ClustalW (Thompson et al. 1994). Highlighted with *red boxes* are the conserved residues Ala8, Ala14, Pro4, Pro5, Pro105, and Pro253 that were sequentially assigned for hVDAC1 in our previous study

The N-terminal region of hVDAC2 is eleven amino acids longer compared to hVDAC1 giving rise to a total number of 31 amino acids before the expected turn prior to β-strand 1 at Gly21. For the sake of simplicity we use in this work the numbering for the hVDAC2 sequence such that it matches the hVDAC1 sequence.

Materials and methods

Solid-state NMR

hVDAC2 was expressed, refolded, and purified according to the protocol described in Engelhardt et al. (2007). For solid-state NMR measurements, the protein was reconstituted into dimyristoyl phosphocholine (DMPC) liposomes at a protein/lipid ratio of 1/50 (mol/mol). Solid-state NMR experiments were conducted using a 4 mm triple-resonance (^{1}H, ^{13}C, ^{15}N) magic-angle spinning (MAS) probe head at a static magnetic field of 20.0 T (Bruker Biospin, Karlsruhe, Germany). The sample temperature was set to +5 °C. An initial ^{1}H–^{13}C cross-polarization (CP) contact time of 600 μs was used. Typical proton field strength for 90° pulses and SPINAL-64 (Fung et al. 2000) decoupling was ~83 kHz. ^{13}C–^{13}C mixing was accomplished by proton-driven spin diffusion (PDSD) for 20 ms, at an MAS frequency of 11 kHz. Spectra were processed in Topspin (Bruker Biospin, Karlsruhe, Germany) and analyzed using Sparky (T. D. Goddard and D. G. Kneller, SPARKY 3, University of California, San Francisco).

Electrophysiology

The artificial lipid bilayer method has been previously described in detail (Benz et al. 1978). In brief, membranes were formed from a solution of 1 % diphytanoylphosphatidylcholine (DiPh-PC; Avanti Polar Lipids, Alabaster, AL) in n-decane across a circular hole (surface area about 0.4 mm^2) dividing two aqueous compartments of a Teflon cell. Both compartments are filled with an unbuffered 1 M KCl solution with a pH of about 6. Two Ag/AgCl electrodes with salt bridges were inserted in both aqueous compartments and switched in series with a voltage source and a Keithley 427 current amplifier. The amplified signal was filtered at 100 Hz, which allowed a reasonable signal to noise ratio and an easy detection of single channels. The output signal of the current amplifier was monitored with a storage oscilloscope and recorded on a strip chart recorder (Rikadenki Electronics, Germany). For single channel conductance experiments a voltage of ±10 mV was applied to the electrode connected to the voltage source. The stepwise increase in membrane conductance following

the addition of hVDAC2 and its mutant in a final concentration of about 100 nM were determined as described previously (Benz et al. 1978). Histograms of current fluctuations were derived from at least 100 upward directed conductance steps. Zero current membrane potential measurements were obtained by establishing a salt gradient across membranes containing about 100 hVDAC2 or Δ(1–31)-hVDAC2 channels as described elsewhere (Benz et al. 1985).

Molecular dynamics simulations

MD simulations were performed using Gromacs 4.0 (Hess et al. 2008) together with the OPLS (Jorgensen 1996) and amber99sb force-fields (Wang et al. 2004), respectively, for the protein, water, and ions. The initial structure of human VDAC2 was modeled with MODELLER (Šali and Blundell 1993) where the crystal structure of murine VDAC1 (Ujwal et al. 2008) (pdb code 3EMN) was used as a template structure. For equilibrium simulations of model structures of WT-hVDAC2, the protein was inserted in simulation boxes of DMPC and water. DMPC parameters were derived from Berger et al. (Berger et al. 1997), and the TIP4P model was used for water (Jorgensen and Madura 1983). Water bond distances and angles were constrained using SETTLE (Miyamoto and Kollman 1992). Electrostatic interactions were calculated explicitly at a distance smaller than 1.0 nm, long-range electrostatic interactions were treated by particle-mesh Ewald summation at every step (Darden et al. 1993). Lennard–Jones interactions were calculated using a cutoff of 1.0 nm. The LINCS algorithm was employed to constrain all protein and lipid bonds (Hess et al. 1997). The simulation temperature was kept constant by weakly ($t = 0.1$ ps) coupling the system to a temperature bath of 320 K using the velocity rescale method (Bussi et al. 2007). The pressure was kept constant by semi-isotropic Berendsen coupling of the system to a pressure bath of 1 bar, separately for the xy- and for the z-direction (Berendsen et al. 1984; Feenstra et al. 1999). An integration time-step of 2 fs was used.

Atom-positional root-mean-square fluctuations (RMSF) over a full period of simulation were calculated after superposition of centers of mass and performing a rotational atom-positional least-squares fit of the trajectory structures on the reference model structure. The secondary structure assignment was done by using the program DSSP, based on the Kabsch–Sander rules (Kabsch and Sander 1983). A conformational clustering analysis was carried out on 10^6 configurations using an atom-positional root-mean-square difference (RMSD) similarity criterion of 0.1 nm for backbone atoms of all and of barrel residues only (based on the homology model) using an algorithm as described in (Daura et al. 1999).

Results and discussion

Similarities and differences between the hVDAC1 and hVDAC2 structures

A proton-driven spin diffusion (PDSD) experiment on reconstituted hVDAC2 recorded with a short mixing time of 20 ms resulted in a spectrum very similar to the one of hVDAC1 (Fig. 2a). However, the hVDAC2 spectrum appears to be broader with fewer sharp and isolated cross-peaks. The obvious resemblance between the two spectra points to structural similarities between the two hVDAC isoforms. In particular, hVDAC2 shows the characteristic pattern of the peaks belonging to the β-barrel which suggests that the barrel fold is conserved between the two isoforms. This result is not unexpected due to the sequence similarity in the barrel part of the protein (Fig. 1).

Due to the observed spectral crowding and the sparse number of isolated peaks in the spectrum of uniformly labeled hVDAC2, we resorted to a forward-labeling scheme with the intent to provide solid structural information about the N-terminus of hVDAC2 from solid-state NMR data. Based on the hVDAC2 sequence we decided to study a Cys, Ile, Phe and Pro (CIFP) forward-labeled sample. By choosing those amino acids we successfully decreased spectral overlap while still being able to obtain structural information about the N-terminal region (Fig. 3).

There are six Pro residues which are conserved between hVDAC1 and hVDAC2 (P4, P5, P105, P136, P229 and P253), and one additional Pro residue in the extra eleven amino-acid sequence at the N-terminus of hVDAC2 (P0). From the six Pro residues of hVDAC1 so far four (P4, P5, P105 and P253) could be assigned by solid-state NMR methods (Schneider et al. 2010). In the spectrum of the CIFP forward-labeled sample in Fig. 3 and the Pro region of the spectrum of the uniformly labeled sample in Fig. 2b, c it is apparent that the Pro cross-peaks in the hVDAC1 and hVDAC2 spectra appear at similar positions. We therefore tentatively assigned the corresponding peaks in the hVDAC2 spectra to P4, P5, P105 and P253. We note that the cross-peaks for P4 are very weak in the spectrum of the uniformly labeled sample but are strong in the spectrum of the forward-labeled sample. Whereas in hVDAC1 no Ile residues are present in the N-terminus, the hVDAC2 sequence contains two positions where Val residues are exchanged to Ile (V3 and V17) (Fig. 1). Indeed, the cross-peaks of V3 and V17 are not observed in the spectra of hVDAC2. In Fig. 3 one can assign at least two cross-peaks to α-helical Ile residues that may be from the N-terminal α-helix. Additional support for an α-helical N-terminus comes from the two conserved Ala residues in the N-terminus (A8 and A14) whose cross peaks appear at similar positions in the spectra of hVDAC1 and hVDAC2

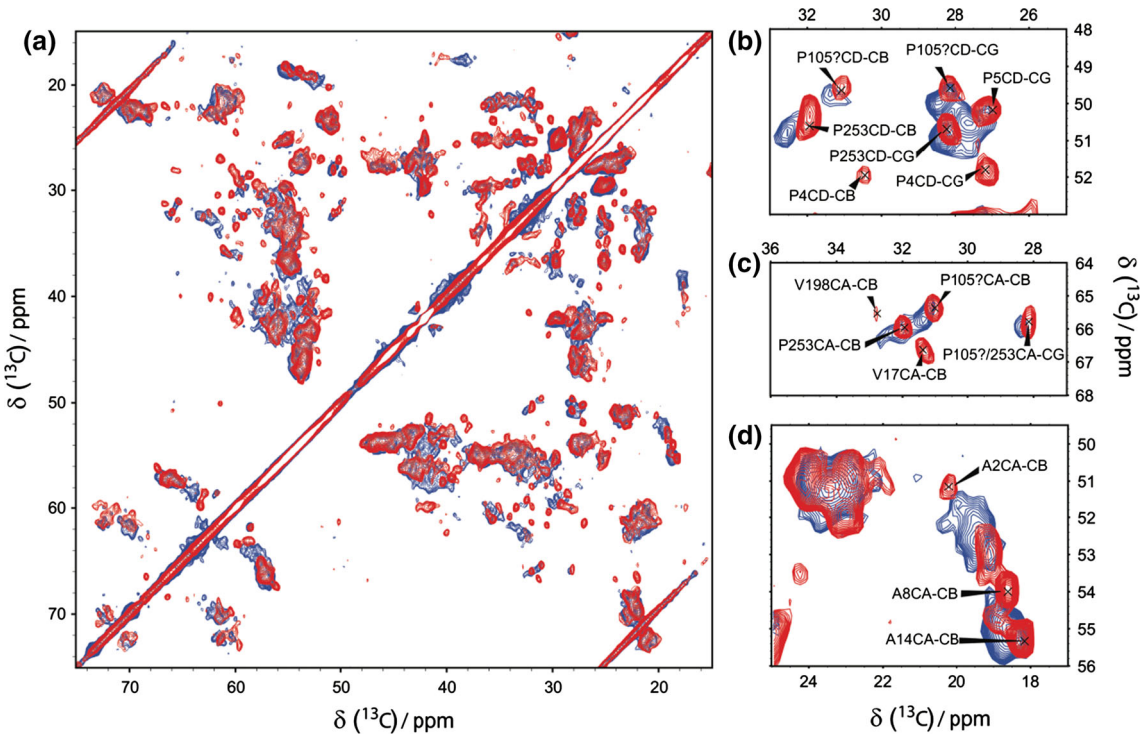

Fig. 2 **a** Overlay of ^{13}C-^{13}C PDSD spectra of full-length u[^{13}C, ^{15}N]-hVDAC1 (*red*) and full-length u[^{13}C, ^{15}N]-hVDAC2 (*blue*) in lipid bilayers recorded on an 850 MHz spectrometer; **b**, **c** excerpts of proline regions, and **d** excerpt of alanine region; displayed assignments correspond to assignments of u[^{13}C, ^{15}N]-hVDAC1 (Schneider et al. 2010)

(Fig. 2c). In summary all available data indicate that the N-terminus of hVDAC2, in the region homologous to hVDAC1, adopts an α-helical conformation similar to the one found in hVDAC1.

Electrophysiology measurements on hVDAC2

The addition of the low concentration (100 ng/ml) of the refolded hVDAC2 protein to lipid bilayers made of DiPhPC/n-decane allowed the resolution of stepwise conductance increases. Figure 4a shows a single channel recording of hVDAC2 at the low voltage of 10 mV 3 min after the addition of the protein to one side (the *cis*-side) of a lipid bilayer membrane. Each step indicated the reconstitution of one channel into the membrane. Most of the steps were directed upwards, which demonstrated that the channels were always in the open state and had a very long lifetime at low voltage. Figure 4b shows a histogram of all conductance steps observed in reconstitution experiments with refolded hVDAC2 in 1 M KCl. The most frequent values for the single channel conductance of hVDAC2 under these conditions were 2 and 4 nS. For both positive and negative transmembrane potentials larger than 30 mV the membrane current decreases exponentially, in agreement with the voltage-dependence typical of VDAC channels (Benz 1994; Colombini 2004). Compared to hVDAC1, however, wt-hVDAC2 has a broader distribution (Zachariae et al. 2012). A broad distribution of conductance states for mouse VDAC2 was already reported before by Xu et al. (1999), although that study did not report the presence of two conductance-state maxima as observed here but only a single conductance of 3.79 ± 0.10 nS.

It was previously shown for *Neurospora crassa* VDAC (ncVDAC) that deletion of most or all of the 20 N-terminal residues leads to more noisy recordings in electrophysiology, affects or abolishes voltage gating, and reduces channel conductance (Popp et al. 1996; Runke et al. 2006). This also applies to hVDAC2 upon deletion of the first 31 amino acids (full N-terminal part) as seen in Fig. 5. Lipid bilayer measurements on a hVDAC2 N-terminal truncation variant (Δ(1–31)-hVDAC2) showed noisy traces, similar to the deletion mutant of hVDAC1 (Δ(1–21)-hVDAC1) (Zachariae et al. 2012) with no apparent voltage gating and the distribution of conductance levels showing a broad maximum between G = 0.5 nS and G = 3.0 nS (Fig. 5). This indicates that for proper hVDAC2 channel functionality the N-terminus is required. Surprisingly, the deletion of the 31 amino acids at the N-terminus had only a minor influence on the selectivity of the hVDAC2 channel. For a five-fold KCl gradient (0.1 vs. 0.5 M) across a DiPhPC/n-decane membrane containing wt-hVDAC2 channels we observed an asymmetry potential of about −11 mV at the

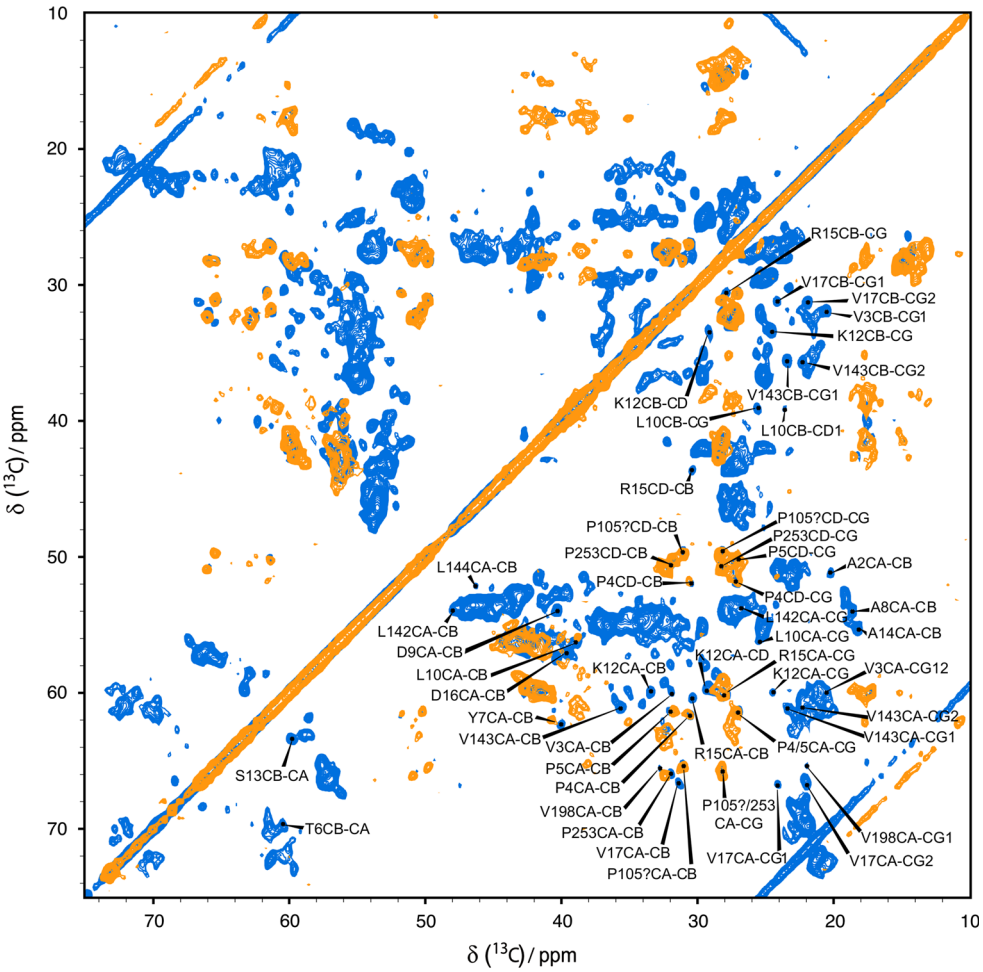

Fig. 3 Overlay of ^{13}C-^{13}C PDSD spectra of full-length u[^{13}C, ^{15}N]-hVDAC1 (*blue*) and CIFP forward-labeled hVDAC2 (*orange*) in lipid bilayers recorded on an 850 MHz spectrometer; displayed assignments correspond to assignments of u[^{13}C, ^{15}N]-hVDAC1 (Schneider et al. 2010)

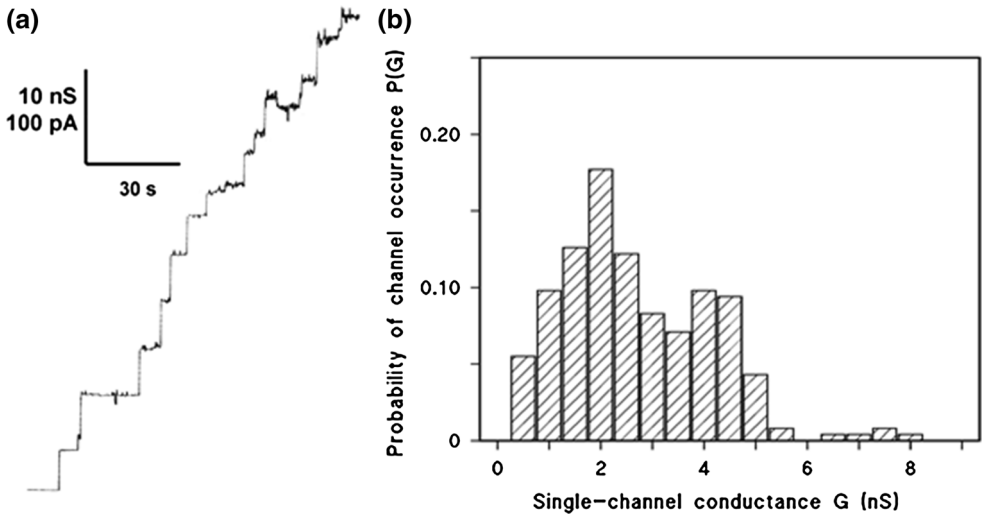

Fig. 4 Lipid bilayer measurements on WT-hVDAC2. **a** Single channel recording of a DiPhPC/n-decane membrane after the addition of 100 ng/ml refolded hVDAC2 to the aqueous phase containing 1 M KCl, pH 6. The applied membrane potential was 10 mV; T = 20 °C. Note that from the reconstituted 13 channels (all used for the histogram in (**b**) only one channel closed during the time of the recording. **b** Histogram of the conductance steps measured after reconstitution of the refolded hVDAC2 into black lipid bilayer membranes; same conditions as in A. The probability P(G) for the occurrence of a given conductivity unit was calculated by dividing the number of fluctuations with a given conductance increment by the total number of conductance fluctuations. The most frequent single channel conductance was about 2 nS and 4 nS for in total 254 channels from in total 5 different DiPhPC/n-decane membranes

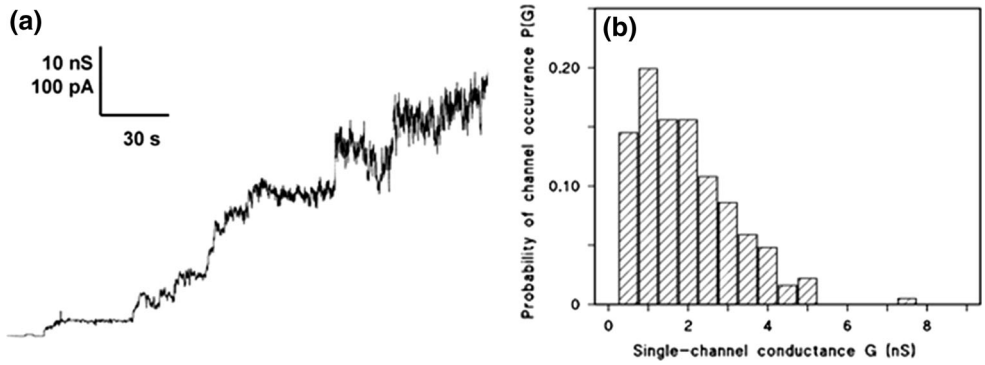

Fig. 5 Lipid bilayer measurements on the deletion mutant Δ(1–31)-hVDAC2. **a** Single channel recording of a DiPhPC/n-decane membrane after the addition of 100 ng/ml refolded deletion mutant Δ(1–31)-hVDAC2 to the aqueous phase containing 1 M KCl, pH 6. The applied membrane potential was 10 mV; T = 20 °C. **b** Histogram of the conductance steps measured after reconstitution of the refolded deletion mutant Δ(1–31)-hVDAC2 into black lipid bilayer membranes; same conditions as in (**a**). The probability P(G) for the occurrence of a given conductivity unit was calculated by dividing the number of fluctuations with a given conductance increment by the total number of conductance fluctuations. The most frequent single channel conductance was about 1.5 nS for in total 212 single insertions from in total 10 different DiPhPC/n-decane membranes

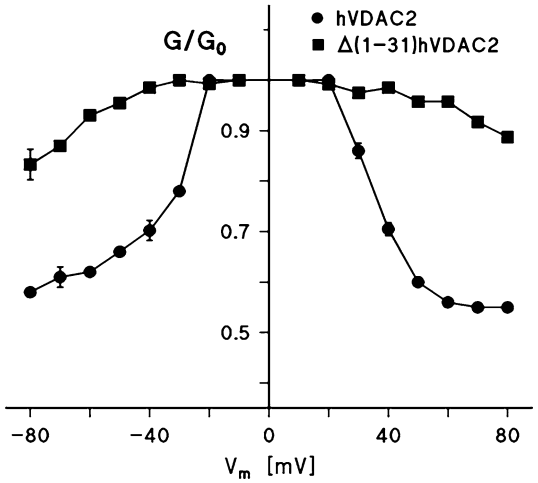

Fig. 6 Voltage dependence of hVDAC2 and the deletion mutant Δ(1–31)-hVDAC2 when the proteins were added in a final concentration of 100 ng/ml to the *cis*-side of DiPhPC/n-decane membranes immersed in 1 M KCl, pH 6; T = 20 °C. Shown are ratios of the conductance G at a given membrane potential (Vm) divided by the conductance G0 at 10 mV as a function of the membrane potential Vm. *Circles* refolded hVDAC1; *squares* refolded Δ(1–31)-hVDAC2. The membrane potential always refers to the cis-side of the membrane. Mean ± SD of three membranes are shown for each hVDAC2 variant

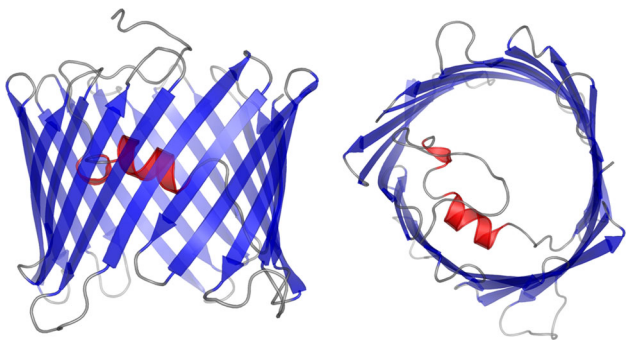

Fig. 7 Homology model of human VDAC2 generated with MODELLER (Šali and Blundell 1993). The structure of murine VDAC1 (Ujwal et al. 2008) was used as a template

more dilute side indicating that the ratio of permeability of chloride divided by permeability of potassium P_{Cl}/P_K was about two. The selectivity of the hVDAC2 N-terminal truncation variant (Δ(1–31)-hVDAC2) was with $P_{Cl}/P_K = 1.8$ (asymmetry potential −9.9 mV at the more diluted side) only little smaller indicating that the amino acids 1–31 at the N-terminus had an only small impact on channel selectivity of hVDAC2 if any.

In single channel recordings the channel formed by hVDAC2 exhibited some flickering at higher voltages, i.e. it showed transitions between open and closed configurations that were not observed at low voltage. This could be caused by voltage dependent closing of the hVDAC2 channel, which is typical for hVDAC channels (Benz 1994; Colombini 2004; Zachariae et al. 2012). To study this effect in more detail we increased the voltage across the membranes in multi-channel experiments. We applied different negative and positive potentials (with respect to the cis side, the side where hVDAC2 was added) to the membrane, starting from ±10 mV. Then we repeated the experiment with ±20, ±30, ±40 up to ±80 mV. The membrane current started to decrease for both polarities when the voltage at the *cis* side exceeded ±20 mV. The data of the voltage dependence experiments were analyzed in the following way: the membrane conductance (G) as a function of voltage, Vm, was measured when the opening and closing of channels reached an equilibrium, i.e. after the exponential decay of the membrane current following the voltage step Vm. G was divided by the initial value of the conductance (G0, which was a linear function of the

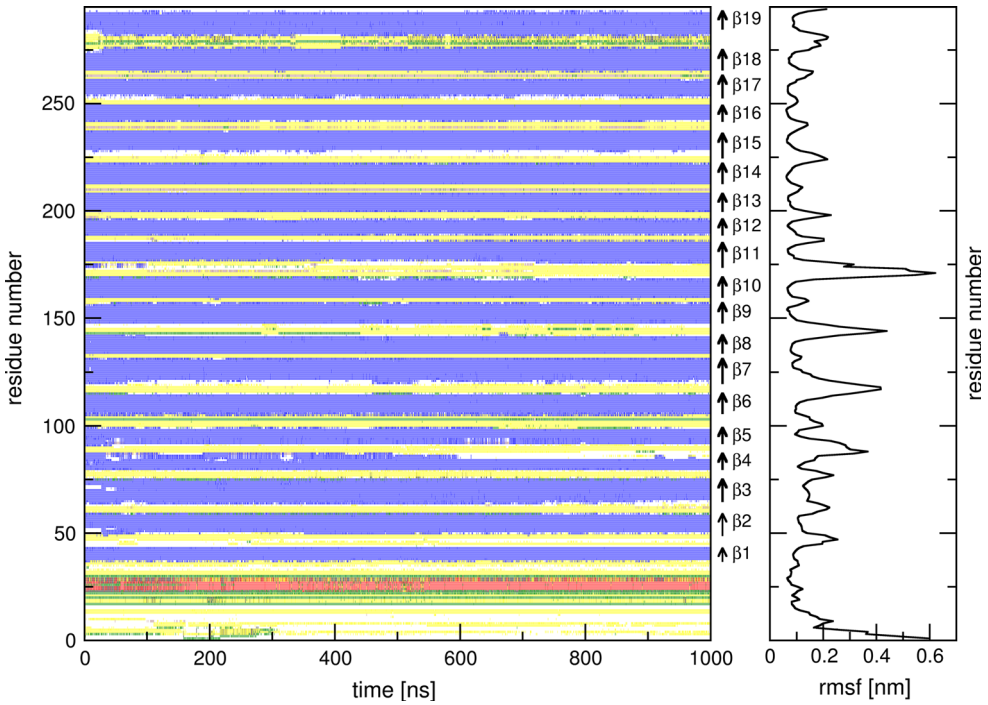

Fig. 8 Secondary structure analysis (DSSP) and Cα root mean square fluctuation (RMSF) analysis performed on a 1 μs long MD simulation. The main secondary structure comprises a 19-stranded β-barrel and an N-terminal α-helix. A *red line* represents an α-helix, *green* turn, *blue* β-strand, *yellow* bend, and *black* β-bridge

voltage) obtained immediately after the onset of the voltage. The data in Fig. 6 corresponded to the approximately symmetric voltage dependence of hVDAC2 [full points; mean of three experiments (±SD)] when hVDAC2 was added to one side of the membrane. Similar experiments were also performed with the N-terminal truncation variant (Δ(1–31)-hVDAC2) of hVDAC2 [full squares in Fig. 6; mean of three experiments (±SD)]. Only minor channel gating was observed in this case indicating that the N-terminus of VDAC-proteins plays a major role in voltage-dependent channel gating and its deletion resulted in almost complete absence of gating (see Fig. 6).

Molecular dynamics simulations of hVDAC2 in a DMPC bilayer

In parallel to the solid-state NMR experiments we performed a molecular dynamics study on a homology model of hVDAC2. The homology model was created with MODELLER (Šali and Blundell 1993) where the crystal structure of murine VDAC1 (Ujwal et al. 2008) was used as the template (Fig. 7). The system was embedded into a DMPC lipid bilayer, which was equilibrated for 10 ns, and the final simulation box was filled with explicit water (see "Materials and methods" section). After 5 ns of equilibration time, the total time of simulation was 1 μs.

Secondary structure analysis (DSSP) and root-mean-square fluctuation (RMSF) analysis on the full 1 μs simulation shows that the 19 stranded β-barrel fold was present throughout the full time of simulation. The RMSF analysis shows increased dynamics in all the loop regions and also for the first eleven residues—which were modeled as a random coil due to the absence of structural information for this region. The N-terminal α-helix expected from homology modeling and solid-state NMR results (see above) was present during the entire simulation time (Fig. 8). From the RMSF analysis one can see that over the full simulation time, β-strands of the barrel show a small level of fluctuation except for β-strands 2–6. High flexibility of the β-barrel was also observed for β-strands 2–7 of hVDAC1 (Villinger et al. 2010). The first eleven residues did not adopt any specific secondary structure during the simulation (Fig. 8). Conformational clustering analysis did not reveal any cluster of conformations where the helix was not positioned as in the initial structure. This was further confirmed by a distance analysis between Leu10 and Val143 (data not shown).

Conclusion

In the present work our goal was to investigate similarities and differences between hVDAC1 and hVDAC2 by means of solid-state NMR, electrophysiology, and molecular dynamics simulations. Clear similarities between hVDAC1 and hVDAC2 solid-state NMR spectra indicate that both isoforms do fold into the same β-barrel structure. The stronger broadening of resonance signals in hVDAC2 spectra as compared to hVDAC1 indicates a higher degree of conformational heterogeneity of hVDAC2. This is also reflected in broader conductance level distributions found for hVDAC2 in this study compared to sharp distributions

previously observed for hVDAC1 (Schneider et al. 2010). Data obtained on a CIFP forward–labeled sample indicate that the hVDAC2 N-terminus adopts an α-helical conformation in the region homologous to hVDAC1. Our results are in agreement with the recent structure of zfVDAC2 solved by Abramson and coworkers who found a strong structural similarity between zfVDAC2 and mVDAC1 (Schredelseker et al. 2014). The observed structural heterogeneity of hVDAC2 in lipid bilayers as identified in this study and also in a previous study by McDermott and coworkers (Bauer et al. 2011) may explain the fact that so far crystallization trials on hVDAC2 remained unsuccessful. Results from MD simulations corroborate the experimental data: a long 1 μs simulation of a homology model indicates a very stable fold, in particular of the N-terminal α-helix, and shows dynamics of the first 6 β-strands, similar to results obtained for hVDAC1. The first eleven residues remain disordered throughout the course of the simulation but we cannot exclude that they adopt a more ordered conformation in the context of the full length protein as the homology model used in the simulation was based on the mVDAC1 structure that doesn't contain these first eleven residues.

Acknowledgments We thank B. Angerstein for expert technical assistance and R. Briones for help in the initial stages of the project concerning GROMACS. This work was supported by the Max Planck Society, the Leibniz-Institut für Molekulare Pharmakologie, the ERC (grant agreement number 282008 to M.Z.), the DFG (Collaborative research center 803 to A.L., C.G., and M.Z. and Emmy Noether Fellowship to A.L.) and by a Marie Curie fellowship within the 7th EU Framework Program to Z.G.

References

Anflous K, Armstrong DD, Craigen WJ (2001) Altered mitochondrial sensitivity for ADP and maintenance of creatine-stimulated respiration in oxidative striated muscles from VDAC1-deficient mice. J Biol Chem 276:1954–1960. doi:10.1074/jbc.M006587200

Bauer AJ, Gieschler S, Lemberg KM et al (2011) Functional model of metabolite gating by human voltage-dependent anion channel 2. Biochemistry 50:3408–3410. doi:10.1021/bi2003247

Bayrhuber M, Meins T, Habeck M et al (2008) Structure of the human voltage-dependent anion channel. Proc Natl Acad Sci USA 105:15370–15375. doi:10.1073/pnas.0808115105

Benz R (1994) Permeation of hydrophilic solutes through mitochondrial outer membranes: review on mitochondrial porins. Biochim Biophys Acta 1197:167–196

Benz R, Janko K, Boos W, Läuger P (1978) Formation of large, ion-permeable membrane channels by the matrix protein (porin) of *Escherichia coli*. Biochim Biophys Acta (BBA) 511:305–319

Benz R, Schmid A, Hancock R (1985) Ion selectivity of gram-negative bacterial porins. J Bacteriol 162:722–727

Berendsen HJC, Postma JPM, van Gunsteren WF et al (1984) Molecular dynamics with coupling to an external bath. J Chem Phys 81:3684. doi:10.1063/1.448118

Berger O, Edholm O, Jähnig F (1997) Molecular dynamics simulations of a fluid bilayer of dipalmitoylphosphatidylcholine at full hydration, constant pressure, and constant temperature. Biophys J 72:2002–2013. doi:10.1016/S0006-3495(97)78845-3

Blachly-Dyson E, Song J (1997) Multicopy suppressors of phenotypes resulting from the absence of yeast VDAC encode a VDAC-like protein. Mol Cell Biochem 17:5727–5738

Blachly-Dyson E, Zambronicz EB, Yu WH et al (1993) Cloning and functional expression in yeast of two human isoforms of the outer mitochondrial membrane channel, the voltage-dependent anion channel. J Biol Chem 268:1835–1841

Bussi G, Donadio D, Parrinello M (2007) Canonical sampling through velocity rescaling. J Chem Phys 126:014101. doi:10.1063/1.2408420

Cheng EHY, Sheiko TV, Fisher JK et al (2003) VDAC2 inhibits BAK activation and mitochondrial apoptosis. Science 301:513–517. doi:10.1126/science.1083995

Choudhary OP, Paz A, Adelman JL et al (2014) Structure-guided simulations illuminate the mechanism of ATP transport through VDAC1. Nat Struct Mol Biol 21:626–632. doi:10.1038/nsmb.2841

Colombini M (1980) Pore Size and Properties of Channels from Mitoehondria Isolated from Neurospora crassa. J MembrBiol 53:79–84

Colombini M (2004) VDAC: the channel at the interface between mitochondria and the cytosol. Mol Cell Biochem 256–257:107–115

Darden T, York D, Pedersen L (1993) Particle mesh Ewald: an N·log(N) method for Ewald sums in large systems. J Chem Phys 98:10089. doi:10.1063/1.464397

Daura X, Gademann K, Jaun B et al (1999) Peptide folding: when simulation meets experiment. Angew Chem Int Ed Engl 38:236–240. doi:10.1002/(SICI)1521-3773(19990115)38:1/2<236:AID-ANIE236>3.0.CO;2-M

De Pinto V, Tomasello F, Messina A et al (2007) Determination of the conformation of the human VDAC1 N-terminal peptide, a protein moiety essential for the functional properties of the pore. ChemBioChem 8:744–756. doi:10.1002/cbic.200700009

Engelhardt H, Meins T, Poynor M et al (2007) High-level expression, refolding and probing the natural fold of the human voltage-dependent anion channel isoforms I and II. J Membr Biol 216:93–105. doi:10.1007/s00232-007-9038-8

Feenstra KA, Hess B, Berendsen HJC (1999) Improving efficiency of large time-scale molecular dynamics simulations of hydrogen-rich systems. J Comput Chem 20:786–798. doi:10.1002/(SICI)1096-987X(199906)20:8<786:AID-JCC5>3.0.CO;2-B

Fung BM, Khitrina K, Ermolaev K (2000) An improved broadband decoupling sequence for liquid crystals and solids. J Magn Reson 142:97–101. doi:10.1006/jmre.1999.1896

Hess B, Bekker H, Berendsen HJC, Fraaije JGEM (1997) LINCS: a linear constraint solver for molecular simulations. J Comput Chem 18:1463–1472. doi:10.1002/(SICI)1096-987X(199709)18:12<1463:AID-JCC4>3.0.CO;2-H

Hess B, Uppsala S, Lindahl E (2008) GROMACS 4: algorithms for highly efficient, load-balanced, and scalable molecular simulation, pp 435–447

Hiller S, Garces RG, Malia TJ et al (2008) Solution structure of the integral human membrane protein VDAC-1 in detergent micelles. Science 321:1206–1210. doi:10.1126/science.1161302

Jorgensen W (1996) Development and testing of the OPLS all-atom force field on conformational energetics and properties of organic liquids. J Am Chem Soc 118:11225–11236

Jorgensen WL, Madura JD (1983) Solvation and conformation of methanol in water. J Am Chem Soc 105:1407–1413

Kabsch W, Sander C (1983) Dictionary of protein secondary structure: pattern recognition of hydrogen-bonded and geometrical features. Biopolymers 22:2577–2637. doi:10.1002/bip.360221211

Krammer E-M, Homblé F, Prévost M (2011) Concentration dependent ion selectivity in VDAC: a molecular dynamics simulation study. PLoS ONE 6:e27994. doi:10.1371/journal.pone.0027994

Lindén M, Gellerfors P (1983) Hydrodynamic properties of porin isolated from outer membranes of rat liver mitochondria. Biochim Biophys Acta 736:125–129

Miyamoto S, Kollman P (1992) Settle: an analytical version of the SHAKE and RATTLE algorithm for rigid water models. J Comput Chem 13:952–962. doi:10.1002/jcc.540130805

Naghdi S, Varnai P, Hunyady L, Hajnoczky G (2012) The isoform specific N terminus of VDAC2 is dispensable for tBid induced cytochrome C release. Biophys J 102:437a. doi:10.1016/j.bpj.2011.11.2391

Popp B, Court DA, Benz R, Neupert W, Lill R (1996) The role of the N and C termini of recombinant Neurospora mitochondrial porin in channel formation and voltage-dependent gating. J Biol Chem 271:13593–13899

Reina S, Palermo V, Guarnera A et al (2010) Swapping of the N-terminus of VDAC1 with VDAC3 restores full activity of the channel and confers anti-aging features to the cell. FEBS Lett 584:2837–2844. doi:10.1016/j.febslet.2010.04.066

Rostovtseva T, Colombini M (1997) VDAC channels mediate and gate the flow of ATP: implications for the regulation of mitochondrial function. Biophys J 72:1954–1962. doi:10.1016/S0006-3495(97)78841-6

Rui H, Lee KI, Pastor RW, Im W (2011) Molecular dynamics studies of ion permeation in VDAC. Biophys J 100:602–610. doi:10.1016/j.bpj.2010.12.3711

Runke G, Maier E, Summers W et al (2006) Deletion variants of Neurospora mitochondrial porin: electrophysiological and spectroscopic analysis. Biophys J 90:3155–3164. doi:10.1529/biophysj.105.072520

Šali A, Blundell T (1993) Comparative protein modelling by satisfaction of spatial restraints. J Mol Biol 234:779–815

Sampson MJ, Lovell RS, Craigen WJ (1996) Isolation, characterization, and mapping of two mouse mitochondrial voltage-dependent anion channel isoforms. Genomics 33:283–288. doi:10.1006/geno.1996.0193

Sampson MJ, Lovell RS, Craigen WJ (1997) The Murine voltage-dependent anion channel gene family. J Biol Chem 272:18966–18973

Sampson MJ, Decker WK, Beaudet AL et al (2001) Immotile sperm and infertility in mice lacking mitochondrial voltage-dependent anion channel type 3. J Biol Chem 276:39206–39212. doi:10.1074/jbc.M104724200

Schein SJ, Colombini M, Finkelstein A (1976) Reconstitution in planar lipid bilayers of a voltage-dependent anion-selective channel obtained from paramecium mitochondria. J Membr Biol 30:99–120

Schneider R, Etzkorn M, Giller K et al (2010) The native conformation of the human VDAC1 N terminus. Angew Chem Int Ed Engl 49:1882–1885. doi:10.1002/anie.200906241

Schredelseker J, Paz A, López CJ et al (2014) High resolution structure and double electron–electron resonance of the zebrafish voltage-dependent anion channel 2 reveal an oligomeric population. J Biol Chem 289:12566–12577. doi:10.1074/jbc.M113.497438

Smack DP, Colombini M (2014) Voltage-dependent channels found in the membrane fraction of corn mitochondria. 1985:1094–1097

Sorgato MC, Moran O (1993) Channels in mitochondrial membranes: knowns, unknowns, and prospects for the future. Crit Rev Biochem Mol Biol 28:127–171

Teijido O, Rappaport SM, Chamberlin A et al (2014) Acidification affects voltage-dependent anion channel functioning asymmetrically: role of salt bridges. J Biol Chem. doi:10.1074/jbc.M114.576314

Thompson JD, Higgins DG, Gibson TJ (1994) CLUSTAL W: improving the sensitivity of progressive multiple sequence alignment through sequence weighting, position-specific gap penalties and weight matrix choice. Nucleic Acids Res 22:4673–4680

Ujwal R, Cascio D, Colletier J-P et al (2008) The crystal structure of mouse VDAC1 at 2.3 A resolution reveals mechanistic insights into metabolite gating. Proc Natl Acad Sci USA 105:17742–17747. doi:10.1073/pnas.0809634105

Villinger S, Briones R, Giller K et al (2010) Functional dynamics in the voltage-dependent anion channel. Proc Natl Acad Sci USA 107:22546–22551. doi:10.1073/pnas.1012310108

Villinger S, Giller K, Bayrhuber M (2014) Nucleotide interactions of the human voltage-dependent anion channel. J Biol Chem 289:13397–13406. doi:10.1074/jbc.M113.524173

Wang J, Wolf RM, Caldwell JW et al (2004) Development and testing of a general amber force field. J Comput Chem 25:1157–1174. doi:10.1002/jcc.20035

Xu X, Decker W, Sampson M (1999) Mouse VDAC isoforms expressed in yeast: channel properties and their roles in mitochondrial outer membrane permeability. J Membr Biol 170:89–102

Yagoda N, von Rechenberg M, Zaganjor E et al (2007) RAS-RAF-MEK-dependent oxidative cell death involving voltage-dependent anion channels. Nature 447:864–868. doi:10.1038/nature05859

Yamagata H, Shimizu S, Nishida Y et al (2009) Requirement of voltage-dependent anion channel 2 for pro-apoptotic activity of Bax. Oncogene 28:3563–3572. doi:10.1038/onc.2009.213

Yu T-Y, Raschle T, Hiller S, Wagner G (2012) Solution NMR spectroscopic characterization of human VDAC-2 in detergent micelles and lipid bilayer nanodiscs. Biochim Biophys Acta 1818:1562–1569. doi:10.1016/j.bbamem.2011.11.012

Zachariae U, Schneider R, Briones R et al (2012) β-Barrel mobility underlies closure of the voltage-dependent anion channel. Structure 20:1540–1549. doi:10.1016/j.str.2012.06.015